Sensorless Scalar-Controlled Induction Motor Drives With Modified Flux Observer

Chun-Chieh Wang and Chih-Hsing Fang

Abstract—**This paper presents a simple sensorless scalar control algorithm to control the speed of an induction motor. First, a modified flux observer was employed to estimate the stator flux with the voltage command and the feedback current. Then, based on the mathematical model of the induction motor, the slip frequency was calculated, and the frequency of the voltage command was compensated. An auto-boost controller was designed to overcome the decrease in voltages of the stator resistance and to maintain constant stator flux amplitude. To improve the pure integration problem, a highpass filter was installed in the stator flux observer. In this filter, the cut-off frequency is proportional to the voltage frequency; therefore, the phase shift and amplitude degradation of the estimated flux can be corrected easily. Finally, to demonstrate the proposed control algorithm, a PC-based experimental system was constructed in a 1-hp induction motor. Experimental results are presented to validate the effectiveness of our design.**

Index Terms—**Flux observer, induction motor, scalar control, sensorless control, slip estimator.**

I. INTRODUCTION

IN recent years, industrial applications of the inverter-fed induction motor driver have obviously increased. In driver control design, both the scalar and vector control methods are applied extensively. Notably, speed response, operating scope, and speed accuracy of the latter are superior to the former [1], [2]. However, the scalar control method has a simple control structure and is implemented easily, and thus, within general-purpose industrial applications, it is applied broadly. To improve speed control performance of the scalar control method, an encoder or speed tachometer is required to feedback the rotor angle or rotor speed signal and compensate the slip frequency. However, it is expensive and destroys the mechanical robustness of the induction motor.

Recently, sensorless control of the induction motor has been focused on and developed. Many superior sensorless control methods have been proposed [3]–[8]. For example, Bonanno *et al.* [3] employed a parallel structured rotor flux estimator to avoid the pure integration problem as well as correct the phase shift and amplitude degradation of the estimated flux. Schauder [4] applied the model reference adaptive system to estimate the

rotor speed. Based on the cross product of the estimate rotor flux vectors, which is produced by the voltage and the current model, the adaptive law regulates the estimated speed. In addition, Peng *et al.* [5] assumed that the instantaneous reactive power model to design a robust speed estimator, which was robust to both stator resistor variation and pure integration. Kubota and Yang *et al.* [6], [7], applied the full order adaptive observer to estimate motor speed and stator resistor simultaneously. Kubota *et al.* further injected an ac component into the flux current command to estimate the rotor resistor and speed independently. In addition, Lee *et al.* [8] employed the feedback stator current and the stator flux reference to estimate the slip angular frequency and calculate the motor speed. Bose *et al.* [9] replaced the pure integrator of the flux observer with three programmable-cascaded lowpass filters for which the bandwidth is dependent on the electric frequency. Hu *et al.* [10] applied the inner product of the estimate flux and the back electric magnetic force (EMF) to correct the estimated flux value. Finally, Shin *et al.* [11] employed a lowpass filter for which the bandwidth is proportional to the electrical frequency and a correct matrix to estimate the stator flux and rotor speed of the induction motor.

II. INDUCTION MOTOR MODEL

The dynamic model of an induction motor in the general d–q reference frame can be described as [2]

$$\dot{\lambda}_{ds} = V_{ds} - R_s i_{ds} + \omega \lambda_{qs} \tag{1}$$

$$\dot{\lambda}_{qs} = V_{qs} - R_s i_{qs} - \omega \lambda_{ds} \tag{2}$$

$$\dot{\lambda}_{dr} = -\frac{\lambda_{dr}}{\tau_r} + (\omega - \omega_r)\lambda_{qr} + \frac{L_m i_{ds}}{\tau_r} \tag{3}$$

$$\dot{\lambda}_{qr} = -\frac{\lambda_{qr}}{\tau_r} - (\omega - \omega_r)\lambda_{dr} + \frac{L_m i_{qs}}{\tau_r} \tag{4}$$

$$\lambda_{dr} = L_r \frac{\lambda_{ds} - \sigma L_s i_{ds}}{L_m} \tag{5}$$

$$\lambda_{qr} = L_r \frac{\lambda_{qs} - \sigma L_s i_{qs}}{L_m} \tag{6}$$

$$\sigma = 1 - \frac{L_m^2}{L_s L_r}, \quad \tau_r = \frac{L_r}{R_r} \tag{7}$$

where the state variables (V_{ds}, V_{qs}), (i_{ds}, i_{qs}), $(\lambda_{ds}, \lambda_{qs})$, and $(\lambda_{dr}, \lambda_{qr})$, are the stator voltage, the stator current, and the stator and rotor flux, respectively. ω and ω_r are the angular velocity of the coordinate frame and the induction motor, respectively. Furthermore, τ_r and σ represent the rotor time constant and the leakage coefficient. Finally, R_s, R_r, L_s, L_r, and L_m are the stator and rotor resistor and the stator, rotor, and mutual inductance, individually.

C.-C. Wang is with the Department of Electrical Engineering, Ching Yun Institute of Technology, Jung-Li, Taiwan, R.O.C. (e-mail: wangchih@ms42.hinet.net).

C.-H. Fang is with the Department of Electronic and Control Engineering, National Chiao Tung University, Hsinchu, Taiwan, R.O.C. (e-mail: ericf@itri.org.tw).
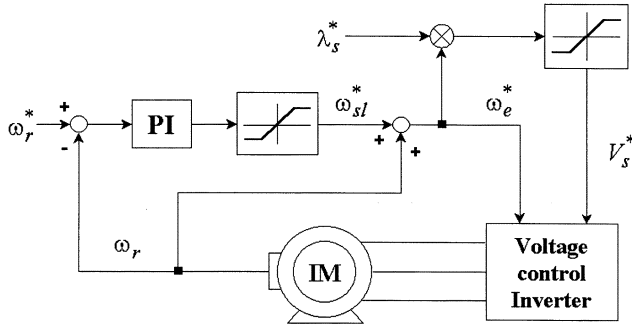
Fig. 1.　Block diagram of the closed-loop scalar control system.

Fig. 2.　Geometric relation of rotor flux in the d^r–q^r reference frame.

III. SCALAR CONTROL

From (1) and (2), the dynamic equations of the stator flux in the synchronous reference frame ($\omega = \omega_e$) can be expressed as

$$\dot{\lambda}_{ds}^e = V_{ds}^e - R_s i_{ds}^e + \omega_e \lambda_{qs}^e \tag{8}$$

$$\dot{\lambda}_{qs}^e = V_{qs}^e - R_s i_{qs}^e - \omega_e \lambda_{ds}^e \tag{9}$$

where ^{e} denotes the variables, which are in the synchronously rotating reference frame, and ω_e is the synchronous angular frequency. Therefore, the steady-state values of stator flux become constant values.

Assume the stator flux vector is in phase with the d^e-axis of the synchronous reference frame and the stator flux amplitude is constant, that is

$$\lambda_{ds}^e = |\bar{\lambda}_s|, \quad \lambda_{qs}^e = 0, \quad \dot{\lambda}_{ds}^e = 0. \tag{10}$$

Substituting (10) into (8) and (9), the stator voltage can be simplified as

$$V_{ds}^e = R_s i_{ds}^e, \tag{11}$$

$$V_{qs}^e = R_s i_{qs}^e + \omega_e |\bar{\lambda}_s|. \tag{12}$$

If the voltage decrease of the stator resistor in (11) and (12) are overlooked, the magnitude correlation between the stator voltage and the stator flux can be approximated as

$$|\bar{V}_s| \approx \omega_e |\bar{\lambda}_s|. \tag{13}$$

For a voltage-fed inverter, to ensure a constant flux value of the induction motor, the ratio of the stator voltage amplitude to the electrical frequency should be kept constant. This is the basic theory of the open-loop scalar control algorithm.

In the open-loop scalar control, the rotor speed of the induction motor varies with the load condition. Therefore, when speed accuracy is required, the closed-loop control strategy will be adopted. In the closed-loop scalar control, the speed PI controller employs the speed error signal to compensate the slip frequency and thus ensures adherence to the speed command. Fig. 1 presents, schematically, the block diagram of a closed-loop scalar control system [2], where the ω_{sl}^* is the compensated slip-frequency, and λ_s^* is the stator flux command.

In Fig. 1, to compensate for the slip frequency, the speed signal must be detected. However, if the slip frequency can be estimated with the stator voltage and current, then the same purpose can be attained without the speed sensor.
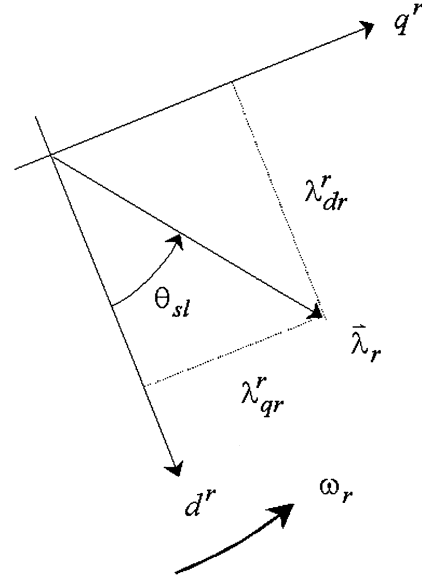
IV. SLIP OBSERVER

From (3) and (4), the dynamic equations of rotor flux in the rotor rotating reference frame ($\omega = \omega_r$) can be expressed as

$$\dot{\lambda}_{dr}^r = -\frac{\lambda_{dr}^r}{\tau_r} + \frac{L_m i_{ds}^r}{\tau_r} \tag{14}$$

$$\dot{\lambda}_{qr}^r = -\frac{\lambda_{qr}^r}{\tau_r} + \frac{L_m i_{qs}^r}{\tau_r} \tag{15}$$

where ^{r} represents the rotor reference frame. The reference axes rotate with ω_r; thus, the rotor flux λ_{dr}^r and λ_{qr}^r will vary with the slip frequency ω_{sl}.

Fig. 2 illustrates the geometric relation of rotor flux in the d^r–q^r reference frame. There is only one constraint on the selection of the d^r- and q^r-axes. That is, the reference axes must rotate with ω_r; therefore, the selection of the axes is not unique. In Fig. 2, the θ_{sl} denotes the slip angle, which is the angle between the rotor flux vector $\bar{\lambda}_r$ and the d^r-axis, that is

$$\theta_{sl} = \tan^{-1}\left(\frac{\lambda_{qr}^r}{\lambda_{dr}^r}\right). \tag{16}$$

The slip frequency equals the time derivative of the slip angle of (16) and can be expressed as

$$\omega_{sl} = \frac{d}{dt}\theta_{sl} = \frac{\lambda_{dr}^r \dot{\lambda}_{qr}^r - \lambda_{qr}^r \dot{\lambda}_{dr}^r}{\lambda_{dr}^{r2} + \lambda_{qr}^{r2}}. \tag{17}$$

Substitute (14) and (15) into (17), and the slip frequency can be simplified as

$$\omega_{sl} = \frac{L_m}{\tau_r}\frac{\lambda_{dr}^r i_{qs}^r - \lambda_{qr}^r i_{ds}^r}{\lambda_{dr}^{r2} + \lambda_{qr}^{r2}} = \frac{L_m}{\tau_r}\frac{\bar{\lambda}_r \otimes \bar{i}_s}{\bar{\lambda}_r \circ \bar{\lambda}_r} \tag{18}$$

where $\otimes$ and $\circ$ denote the cross product and inner product, respectively. Substitute (5) and (6) into (18), and the slip frequency can be rewritten as

$$\omega_{sl} = \frac{L_m^2}{L_r^2}\frac{R_r \bar{\lambda}_s \otimes \bar{i}_s}{(\bar{\lambda}_s - \sigma L_s \bar{i}_s) \circ (\bar{\lambda}_s - \sigma L_s \bar{i}_s)}. \tag{19}$$

The calculations of the cross product and inner product with rotor reference frame or stationary reference frame in (19) are identical. Thus, the estimated stator flux in the stationary reference frame can be applied to calculate the slip frequency.

V. STATOR FLUX OBSERVER

From (1) and (2), the dynamic equation of the stator flux in stationary reference frame ($\omega = 0$) can be expressed as

$$\dot{\lambda}_{ds}^s = e_{ds}^s = V_{ds}^s - R_s i_{ds}^s \tag{20}$$

$$\dot{\lambda}_{qs}^s = e_{qs}^s = V_{qs}^s - R_s i_{qs}^s \tag{21}$$

where ^{s} represents the stationary reference frame, and the e_{ds}^s and e_{qs}^s denote the d^s-axis and q^s-axis back EMF, respectively. From (20) and (21), the open-loop stator flux estimator can be designed as

$$\dot{\hat{\lambda}}_{ds}^s = \hat{e}_{ds}^s = V_{ds}^s - R_s i_{ds}^s \tag{22}$$

$$\dot{\hat{\lambda}}_{qs}^s = \hat{e}_{qs}^s = V_{qs}^s - R_s i_{qs}^s \tag{23}$$

where $\hat{\ }$ is the estimated value.

In (22) and (23), pure integrators are applied to estimate the stator flux. Notably, initial value error and dc-offset problems exist herein. To improve these problems, the observer used to cascade a highpass filter [3], and the equations can be expressed as

$$\dot{\hat{\lambda}}_{ds}^f = -\omega_c \hat{\lambda}_{ds}^f + \hat{e}_{ds}^s \tag{24}$$

$$\dot{\hat{\lambda}}_{qs}^f = -\omega_c \hat{\lambda}_{qs}^f + \hat{e}_{qs}^s \tag{25}$$

where $\hat{\lambda}_{ds}^f$ and $\hat{\lambda}_{qs}^f$ are the d^s- and q^s-axes estimated flux with highpass filter, respectively, and ω_c is the cut-off frequency of the filter.

Assume the real stator flux can be expressed as

$$\lambda_{ds}^s = \lambda_s \cdot \cos(\omega_e t) \tag{26}$$

$$\lambda_{qs}^s = \lambda_s \cdot \sin(\omega_e t) \tag{27}$$

where λ_s is the stator flux amplitude, and ω_e is the electrical frequency.

Substituting (26) and (27) into (20) and (21), the real back EMF can be expressed as

$$e_{ds}^s = -\omega_e \lambda_s \cdot \sin(\omega_e t) \tag{28}$$

$$e_{qs}^s = \omega_e \lambda_s \cdot \cos(\omega_e t). \tag{29}$$

To implement the stator flux estimator (24) and (25), we need to measure the stator current. In general, the feedback signal will be polluted by the dc offset; therefore, it is reasonable to describe the estimated back EMF $\hat{e}_{ds}^s$ and $\hat{e}_{qs}^s$ as

$$\hat{e}_{ds}^s = -\omega_e \lambda_s \cdot \sin(\omega_e t) + v_{\text{off}} \tag{30}$$

$$\hat{e}_{qs}^s = \omega_e \lambda_s \cdot \cos(\omega_e t) + v_{\text{off}} \tag{31}$$

where v_{off} is the dc offset of the feedback signals.

Substituting (30) and (31) into (24) and (25), the estimated flux $\hat{\lambda}_{ds}^f$ and $\hat{\lambda}_{qs}^f$ can be expressed as

$$\hat{\lambda}_{ds}^f = k_d \cdot e^{-\omega_c t} + \frac{v_{\text{off}}}{\omega_c} + A_f \cdot \lambda_s \cdot \cos(\omega_e t + \Delta\varphi) \tag{32}$$

$$\hat{\lambda}_{qs}^f = k_q \cdot e^{-\omega_c t} + \frac{v_{\text{off}}}{\omega_c} + A_f \cdot \lambda_s \cdot \sin(\omega_e t + \Delta\varphi) \tag{33}$$
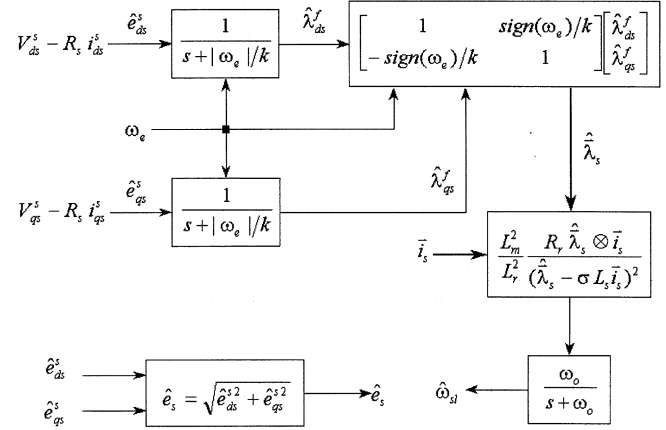

Fig. 3. Block diagram of the stator flux and slip frequency estimator with an accurate matrix.
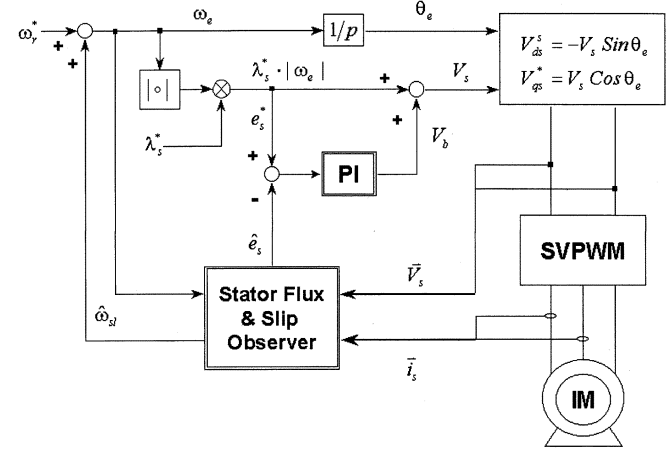

Fig. 4. Overall block diagram of the proposed sensorless scalar control system.

where k_d and k_q are constant values, which correlate with the initial values and dc offset, and A_f and $\Delta\varphi$ are the amplitude attenuation ratio and phase shift between the estimated flux and the real flux and can be expressed as

$$A_f = \frac{|\omega_e|}{\sqrt{\omega_e^2 + \omega_c^2}}, \quad \Delta\varphi = \tan^{-1}\left(\frac{\omega_c}{\omega_e}\right). \tag{34}$$

Comparing (32) and (33) with (26) and (27), we expect a large ω_c to reduce the effects of the initial value errors and dc offset and a small ω_c to increase the ratio of A_f. To balance these two requests, we adopt the estimator structure proposed in [11] to estimate the stator flux, in which the cut-off frequency of the highpass filter is proportional to the electrical frequency, i.e.,

$$\omega_c = \frac{\omega_e}{k}. \tag{35}$$

Substituting (35) into (34), the amplitude attenuation ratio and phase shift can be simplified as

$$A_f = \frac{k}{\sqrt{k^2 + 1}}, \quad \Delta\varphi = \text{sign}(\omega_e) \cdot \tan^{-1}\left(\frac{1}{k}\right). \tag{36}$$

The A_f and $\Delta\varphi$ in (36) are both constant. Therefore, the estimated stator flux can be corrected easily with a constant matrix. Fig. 3 presents the black diagram of the stator flux and slip frequency estimator. In Fig. 3, the $\hat{e}_s$ denotes the amplitude of the
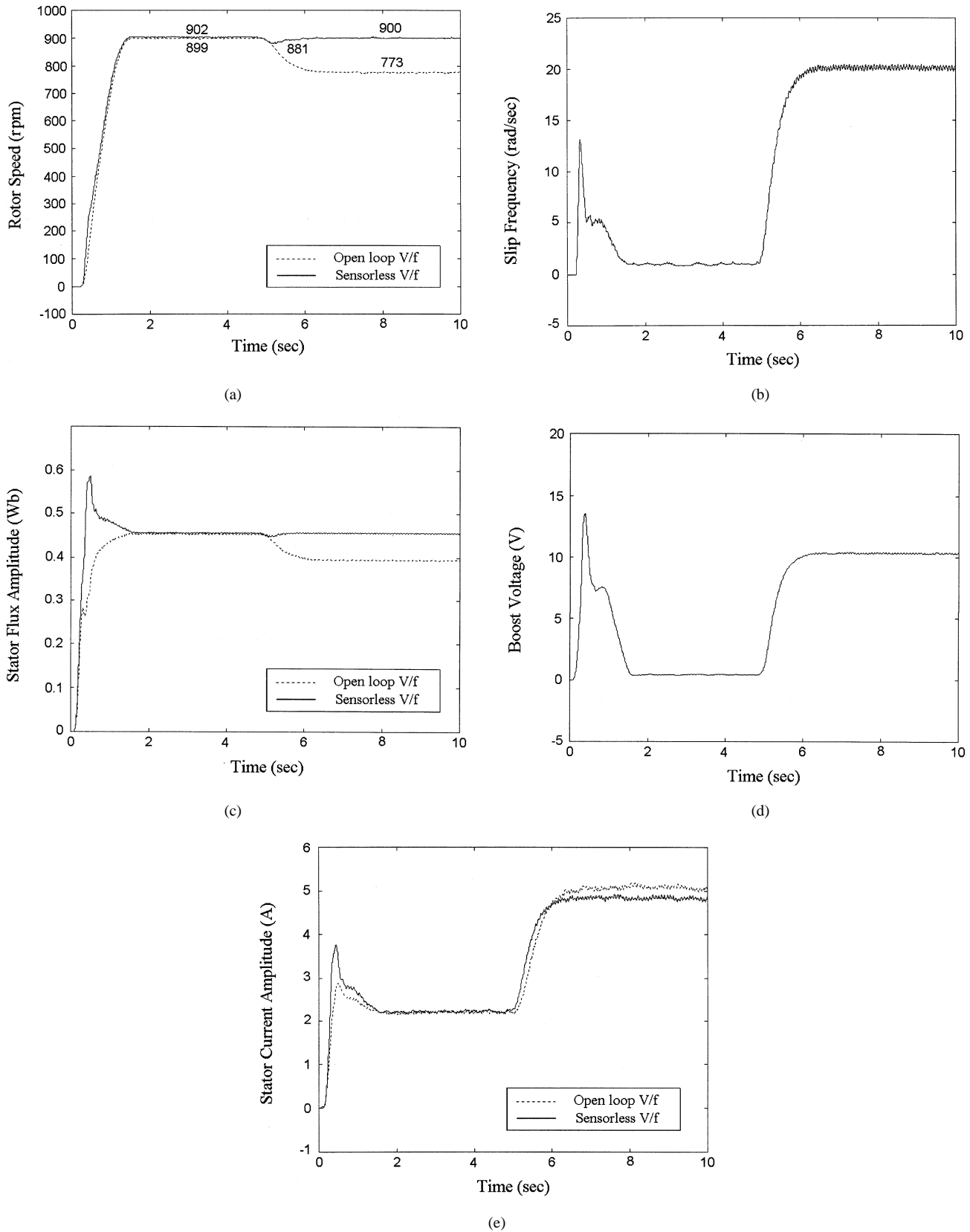
Fig. 5.   Experimental results of the open-loop scalar control method and the proposed sensorless scalar control method at $\omega_r^* = 900$ r/min with a load change from no load to the rated load. (a) Speed. (b) Slip. (c) Amplitude of stator flux. (d) Boost voltage. (e) Amplitude of stator current.

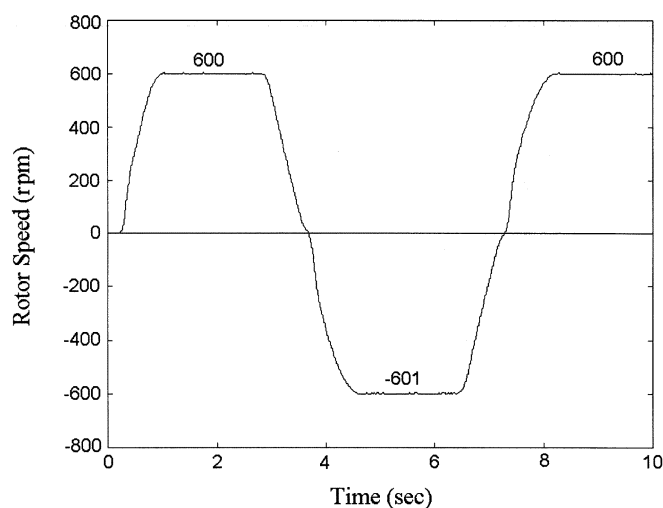back EMF, which will be applied to control the amplitude of the stator flux within the boost controller. To keep the amplitude ratio A_f large enough, such as 0.95, the value of k in (35) is selected as 3 in the following experiments.
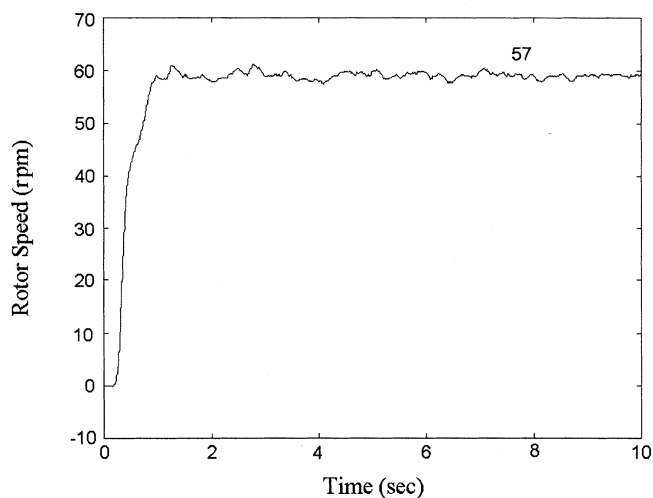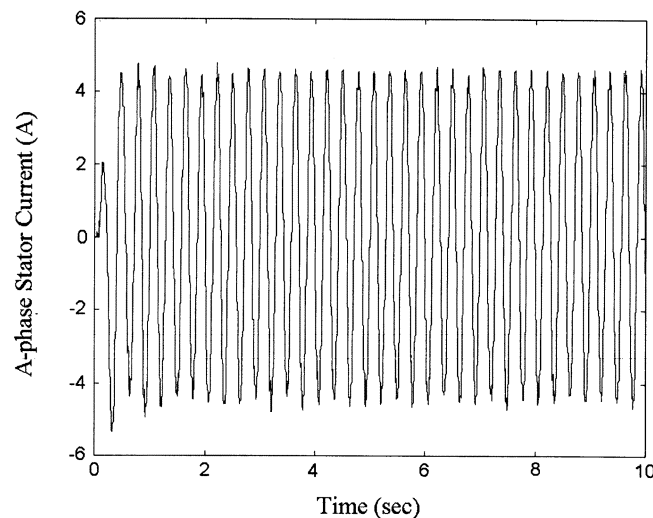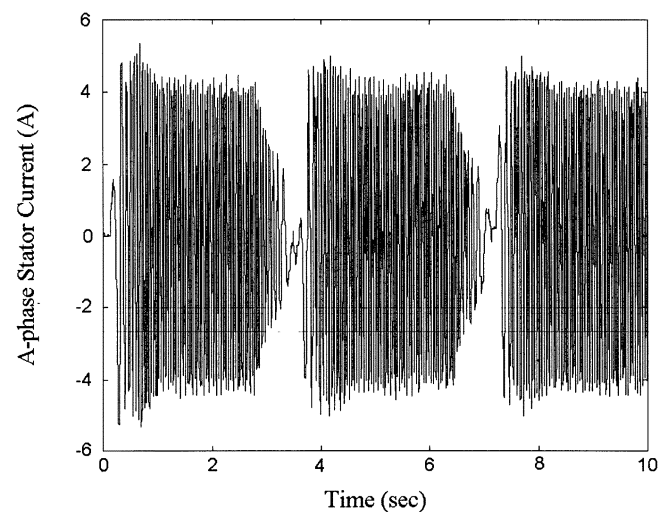
(a)

(b)

Fig. 6. Speed and A-phase current waveforms of the proposed sensorless control method under the rated load at $\omega_r^* = 60$ r/min.

(a)

(b)

Fig. 7. Speed and A-phase current waveforms of the proposed sensorless control method during speed reversal operation ($\omega_r^* = \pm 600$ r/min) and under the rated load condition.

VI. EXPERIMENTAL RESULTS

Fig. 4 illustrates schematically the overall block diagram of the proposed sensorless scalar control for the induction motor drive. In Fig. 4, a boost voltage controller is applied to control the flux amplitude. To reduce the effect of the estimated flux error on the flux control, the back EMF error is applied to regulate the boost voltage. Furthermore, to investigate the feature of the proposed controller in Fig. 4, an experimental design is assembled. The primary components of this design are one 586-K personal computer (PC) with a servo control card insert into its ISA bus, which has eight 12 bit A/D converters, four D/A converters, and a 16-bit encoder counter. In addition, there is a ramp comparison voltage-fed inverter, a 1-hp, 220-V, 3.4-A, and 1700 r/min induction motor with a 1000 pulses/rev optical encoder, and a magnetic powder brake system to simulate the mechanical load. The sampling period of the control program was selected as 0.5 ms.

Fig. 5 presents the experimental results of the open-loop scalar control method and the proposed sensorless scalar control method at $\omega_r^* = 900$ r/min with a load increased from no load to the rated load. In a no-load condition, both control

methods display commendable speed accuracy [see Fig. 5(a)]. Alternately, when the rated load is applied to the rotor axis, a massive speed error of nearly 127 r/min occurs due to the open-loop scalar control method. However, as depicted in Fig. 5(b), the proposed sensorless scalar control method estimates the slip frequency and, thus, compensates the electrical frequency command. Therefore, as Fig. 5(a) illustrates, when the load fluctuates, speed accuracy remains intact. In the proposed sensorless control method, when the load fluctuates, the auto-boost controller regulates the boost voltage and maintains a constant flux [see Fig. 5(c) and (d)]. Furthermore, when a rated load is applied, the stator flux amplitude of the open-loop scalar control method is decreased, and thus, additional stator current is required to produce the same torque, as demonstrated in Fig. 5(e). In addition, Fig. 6 depicts the speed and the A-phase current waveforms of the proposed sensorless control method under the rated load at $\omega_r^* = 60$ r/min. Fig. 6(a) presents an acceptable speed response, and although a small oscillation occurs, the stead state error is maintained at approximately 3 r/min. Fig. 7
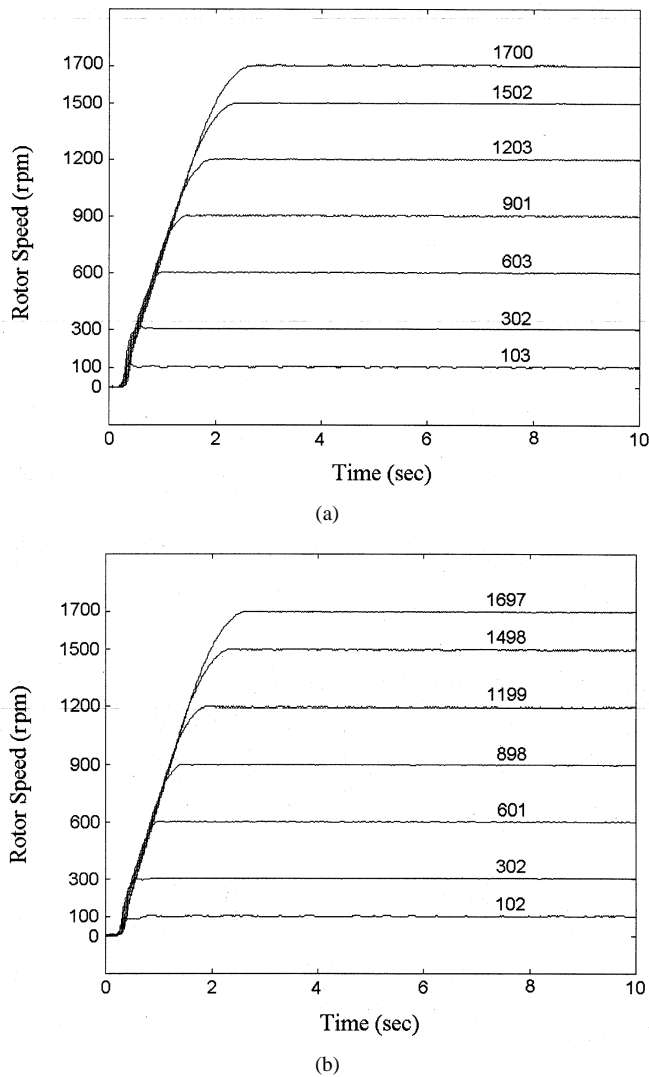
Fig. 8. Measured speed response of the speed reference at 100, 300, 600, 900, 1200, 1500, and 1700 r/min for the sensorless scalar controller under. (a) No load. (b) Full load.

displays the experimental waveforms of the proposed sensorless control method during speed reversal operation and subjected to the rated load condition. In this instance, although the speed reference varies from $+600$ r/min to -600 r/min, it returns to $+600$ r/min. Notably, a stable four-quadrant operation is obtained [see Fig. 7(a)]. Fig. 8 depicts the speed response of the proposed method at various speed references under no load and at the rated load condition. Excellent speed control response is evident in these experimental results. In addition, the steady-state speed error remained less than 5 r/min [see Fig. 8(a) and (b)].

VII. CONCLUSION

In this study, a very simple sensorless scalar control algorithm for the induction motor has been proposed. First, based on the mathematical model of the induction motor, a modified flux observer and a corrected matrix are employed to estimate the stator flux and calculate the slip frequency. Then, to regulate motor speed, the estimated slip frequency was added to the scalar con-

trol method. In the proposed control structure, an auto-boost controller is applied to maintain a constant stator flux amplitude. Finally, to demonstrate the proposed control algorithm in a 1-hp induction motor, a PC-based experimental system was constructed. Experimental results confirm the efficiency of the proposed algorithm for induction motor drives.

REFERENCES

[1] P. Vas, *Vector Control of AC Machines*. New York: Clarendon, 1990.
[2] B. K. Bose, *Power Electronics and AC Drives*. Englewood Cliffs, NJ: Prentice-Hall, 1986.
[3] C. J. Bonanno, L. Zhen, and L. Xu, "A direct field oriented induction machine drive with robust flux estimator for position sensorless control," in *Proc. IEEE-IAS Annu. Meeting*, 1995, pp. 166–173.
[4] C. Schauder, "Adaptive speed identification for vector control of induction motors without rotational transducers," *IEEE Trans. Ind. Applicat.*, vol. 28, pp. 1054–1061, Sept./Oct. 1992.
[5] F. Z. Peng and T. Fukao, "Robust speed identification for speed-sensorless vector control of induction motors," *IEEE Trans. Ind. Applicat.*, vol. 30, pp. 1234–1240, Sept./Oct. 1994.
[6] H. Kubota and K. Matsuse, "Speed sensorless field-oriented control of induction motor with rotor resistance adaptation," *IEEE Trans. Ind. Applicat.*, vol. 30, pp. 1219–1224, Sept./Oct. 1994.
[7] G. Yang and T. H. Chin, "Hyperstability of the full-order observer for vector-controlled induction motor drive without speed sensor," *Elect. Eng. Jpn.*, vol. 113, no. 1, pp. 109–118, 1993.
[8] J. S. Lee, T. Takeshita, and N. Matsui, "Stator-flux-oriented sensorless induction motor drive for optimum low-speed performance," *IEEE Trans. Ind. Applicat.*, vol. 330, pp. 1170–1176, Sept./Oct. 1997.
[9] B. K. Bose and N. R. Patel, "A programmable cascaded low-pass filter-based flux synthesis for a stator flux-oriented vector-controlled induction motor drive," *IEEE Trans. Ind. Electron.*, vol. 44, pp. 140–143, Jan. 1997.
[10] J. Hu and B. Wu, "New integration algorithms for estimation motor flux over a wide speed range," in *Proc. IEEE Power Electron. Specialist's Conf.*, 1997, pp. 1075–1081.
[11] M. H. Shin, D. S. Hyun, S. B. Cho, and S. Y. Choe, "An improved stator flux estimation for speed sensorless stator orientation control of induction motors," *IEEE Trans. Power Electron.*, vol. 15, pp. 312–318, Feb. 2000.

Chun-Chieh Wang was born in Taiwan, R.O.C., in 1967. He received the B.S. degree in nuclear engineering from National Tsing Hua University, Hsinchu, Taiwan, in 1990, and the Ph.D. degrees in electrical engineering from National Taiwan Institute of Technology, Taipei, Taiwan, R.O.C., in 1997.

From 1997 to 1999, he was a research scientist at Industrial Technology Research Institute, Hsinchu. Since 1999, he has been with the Department of Electrical Engineering, Ching Yun Institute of Technology, Jung-Li, Taiwan, where he is currently an Assistant Professor. His research interests include adaptive control, variable structure control, and electric motor control.
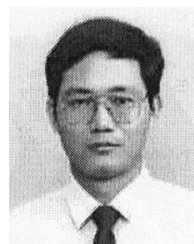
Chih-Hsing Fang was born in Taiwan, R.O.C., in 1956. He received the B.S. degree in automatic control engineering from the Private Feng-Chia University, Taichung, Taiwan, R.O.C., and the M.S. degree in electrical engineering from the Chung-Cheng Institute of Technology, Tao-Yoan, Taiwan, in 1980 and 1987, respectively. He is currently pursuing the Ph.D. degree at the Department of Electronic and Control Engineering, National Chiao Tung University, Hsinchu, Taiwan, R.O.C.

Since 1991, he has been with the Industry Technology Research Institute, Hsinchu, as a design engineer of the induction heating and inverter. His research interests include ac motor drives, control theory applications, and digital signal processing applications in power electronics.